The Journal of Neuroscience, January 1, 2000, 20(1):140–148

Recovery from Open Channel Block by Acetylcholine during Neuromuscular Transmission in Zebrafish

Pascal Legendre,[1] Declan W. Ali,[2] and Pierre Drapeau[2]

[1]*Institut des Neurosciences, Centre National de la Recherche Scientifique, Unité Mixte de Recherche 7624, Université Pierre et Marie Curie, 75252 Paris, France, and* [2]*Center for Research in Neuroscience, Montreal General Hospital Research Institute and McGill University, Montreal, Quebec, Canada H3G 1A4*

At larval zebrafish neuromuscular junctions (NMJs), miniature end plate currents (mEPCs) recorded *in vivo* have an unusually fast time course. We used fast-flow application of acetylcholine (ACh) onto outside-out patches to mimic the effect of synaptic release onto small numbers of ACh receptor channels (AChRs). Positively charged ACh acted at hyperpolarized potentials and at millimolar concentrations as a fast ("flickering") open channel blocker of AChRs. Because of filtering, the open channel block resulted in reduced amplitude of single channel currents. Immediately after brief (1 msec) application (without significant desensitization) of millimolar ACh at hyperpolarized potentials, a slower, transient current appeared because of delayed reversal of the block. This rebound current depended on the ACh concentration and resembled in time course the mEPC. A simple kinetic model of the AChR that includes an open channel-blocking step accounted for our single channel results, as well as the experimentally observed slowing of the time course of mEPCs recorded at a hyperpolarized compared with a depolarized potential. Recovery from AChR block is a novel mechanism of synaptic transmission that may contribute in part at all NMJs.

Key words: fast-flow; single channels; nonstationary kinetics; neuromuscular junction; mEPC; locomotion.

A fundamental issue in synaptic physiology is to determine the relationship between postsynaptic receptor–channel activation kinetics and the time course of the synaptic response elicited upon neurotransmitter release. These issues have been explored extensively at the neuromuscular junction (NMJ) at which quantal release of transmitter was first demonstrated (Fatt and Katz, 1952). In addition, studies of the stationary kinetic properties of nicotinic acetylcholine receptor channels (AChRs) upon prolonged exposure to ACh, particularly at low concentrations, have yielded detailed kinetic models of the channels in a variety of species and show remarkably consistent features (Colquhoun and Sakmann, 1985; Auerbach and Lingle, 1987; Colquhoun and Ogden, 1988; Sine et al., 1990; Liu and Dilger, 1991). At high (millimolar) concentrations, ACh is known to block open AChRs in many (Sine and Steinbach, 1984; Ogden and Colquhoun, 1985; Sine et al., 1990; Liu and Dilger, 1991; Maconochie and Knight, 1992a; Maconochie and Steinbach, 1998) if not all preparations. This is generally believed to limit the effectiveness of AChR activation after vesicular release. Nevertheless, a critical issue is to understand how AChRs respond during brief exposure to the high concentration of ACh released into the synaptic cleft. This can best be performed by nonstationary analysis of AChR kinetics. For example, this approach has revealed the critical role of receptor desensitization in determining the time course and other features of the postsynaptic responses at central synapses (Jones and Westbrook, 1996).

It is particularly important to understand the response properties of AChRs at NMJs at which high rates of release evoke rapid contractions, e.g., during locomotion. In the adult zebrafish, synaptic potentials have been recorded in muscle cells and occur in bursts that are consistent with the fast rate of trunk contractions (20–40 Hz) during swimming (Liu and Westerfield, 1988). This suggests that the speed of neuromuscular transmission must be tightly regulated. Similar high rates of contractions have been observed in zebrafish larvae (Eaton et al., 1977; Saint-Amant and Drapeau, 1998) in which NMJs are formed early during embryogenesis (day 1), and swimming can be evoked at mature rates before hatching (on day 2). In addition, the small size of the muscle cells in zebrafish larvae (up to 5 d) permits high resolution recording of synaptic currents using the patch-clamp technique (Nguyen et al., 1999), which has revealed unusually fast miniature EPCs (mEPCs) with decay time constants of often <1 msec.

To determine the features of AChRs underlying the fast synaptic currents, we examined their properties in outside-out membrane patches (Hamill et al., 1981) during application of high concentrations of ligand (0.1–10 mM ACh) by fast-flow perfusion for periods as brief as 1 msec, as described previously (Legendre, 1998). This allowed us to approximate the effect of synaptic release onto small numbers (10 or fewer) of AChRs. From these results, we developed a simple kinetic model whereby open channel block and recovery from block are major determinants of the time course and other features of the mEPC and suggests a role at other NMJs as well.

Received Aug. 19, 1999; revised Oct. 13, 1999; accepted Oct. 18, 1999.

This work was supported by grants from Institut National de la Santé et de la Recherche Médicale (INSERM) and Association contre les Miopathies of France (P.L.), the Natural Sciences and Engineering Research Council of Canada (NSERC) (P.D.), an NSERC–INSERM Collaborative Exchange (P.L. and P.D., for support of D.W.A.), an NSERC Fellowship (D.W.A.), and a Medical Research Council of Canada–INSERM Visiting Scientist award (P.D.). We thank Dr. N. Leurèche for access to equipment used for some of the whole-cell recordings, Dr. E. Cooper for discussions and comments on this manuscript, and S. Girls for inspiration.

Correspondence should be addressed to Dr. Pierre Drapeau, Department of Neurology, Montreal General Hospital, 1650 Cedar Avenue, Montreal, Quebec, Canada H3G 1A4. E-mail: mcpd@musica.mcgill.ca.

Dr. Ali's present address: Programme in Brain and Behavior, Hospital for Sick Children, 555 University Avenue, Toronto, Ontario, M5G 1X8, Canada.

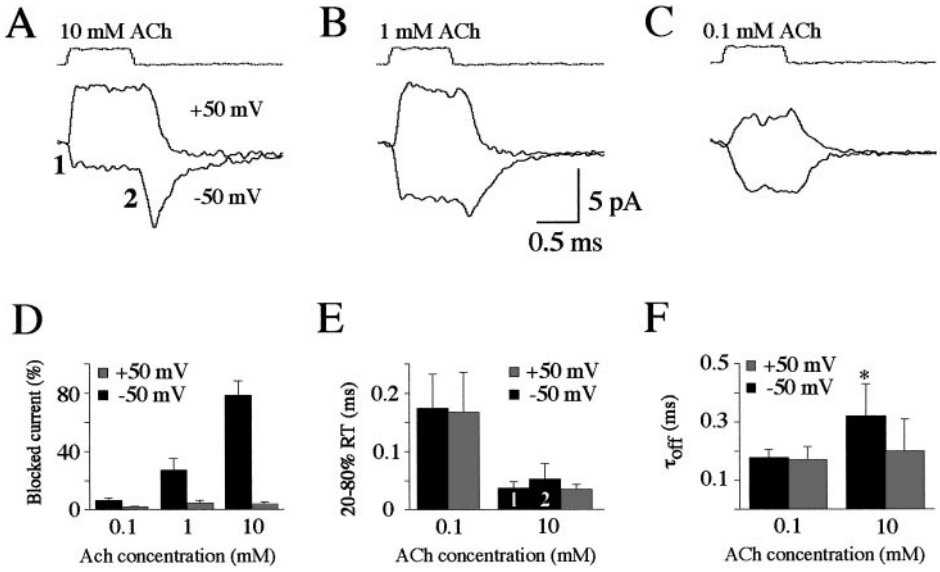

Figure 1. Currents evoked in outside-out patches by fast-flow application of ACh. *A–C*, A series of fast-flow perfusion trials (10–15) separated by 2 sec or more were used to generate an average trace under each condition for the same patch. The *top traces* are recordings of the junctional current recorded from the open pipette upon rupturing the patches at the end of the experiment and indicate the period of ACh application. Current responses during application of 10 (*A*), 1 (*B*), and 0.1 (*C*) mM ACh to the same patch held at +50 (*top traces*) or −50 (*bottom traces*) mV. The *bottom trace* in *A* (at 10 mM ACh) demonstrates an early plateau (*1*), followed by a rebound phase (*2*). *D*, Summary of the extent of current blocked ($n = 5$) at −50 (*black bars*) and +50 (*stippled bars*) mV for patches exposed to 0.1 (*left pair of bars*), 1 (*middle pair of bars*), and 10 (*right pair of bars*) mM ACh. *E*, Summary of the rise times (20–80%) for currents evoked at +50 and −50 mV at either 0.1 (*left pair of bars*) or 10 (*right pair of bars*) mM ACh, including the onset of the plateau phase (*1*) and rebound phase (*2*) observed at −50 mV. *F*, Summary of the exponential time constants (τ_{off}) for deactivation of the currents after termination of the ACh application at +50 and −50 mV at 0.1 (*left pair of bars*) and 10 (*right pair of bars*) mM ACh.

MATERIALS AND METHODS

Whole-cell recording. All procedures were performed in compliance with the guidelines stipulated by the Canadian Council for Animal Care and McGill University. Zebrafish (*Danio rerio*) larvae (3- to 5-d-old) of the Longfin and Tubingen lines were anesthetized in recording solution (see below) containing 0.2% tricaine (MS-222; Sigma, St. Louis, MO). The trunk was severed and pinned on its side through the notochord to the bottom of a Sylgard-coated Petri dish, and the skin was removed using a fine forceps. The preparations were then continuously superfused (~2 ml/min) with oxygenated recording solution that lacked tricaine. The extracellular recording solution was modified from Legendre and Korn (1994) to contain less Ca and more Mg, consisting of (in mM): NaCl 145, KCl 4, $NaHCO_3$ 26, KH_2PO_4 1.25, $CaCl_2$ 0.6, $MgCl_2$ 10, glucose 10, and tetrodotoxin 0.001, adjusted to pH 7.2, 330 mOsm, and bubbled with $95\%O_2$–$5\%CO_2$. Superficial muscle cells were removed to expose the medial surface of deeper muscle cells, but the small size of the NMJs prevented us from directly locating them. We used standard whole-cell recording techniques (Hamill et al., 1981) at room temperature (22°C) from the middle of deep muscle fibers. Patch-clamp electrodes were pulled from thick-walled borosilicate glass and were filled with (in mM): CsCl 130, $MgCl_2$ 2, HEPES 10, EGTA 10, and Na_4ATP 4, pH 7.2, 290 mOsm. The electrode resistance was 1–3 MΩ, and miniature end plate currents (mEPCs) were recorded with an Axopatch 1D or 200B patch clamp (Axon Instruments, Foster City, CA), filtered at 5 kHz (−3 dB), and stored either on the computer or on a digital tape recorder. Data were acquired with pClamp 6.0 software (Axon Instruments) by digitizing at 50 kHz and were analyzed off-line with Axograph 4.0 software (Axon Instruments). The mEPCs were detected as events rising five times above the SD of the noise with a time course resembling that of a well resolved mEPC used as a template. The events were aligned at the corresponding time point of detection. We excluded from analysis a small fraction (<25%) of low-amplitude (less than −50 pA at −50 mV) slow events (rise times of >0.5 msec and decay time constant of >2 msec) thought to result from electrical coupling with neighboring muscle cells (Nguyen et al., 1999). The series resistance (Rs) was 3–10 MΩ, was compensated by 60–95%, and was verified throughout the recordings. Typically, mEPCs were recorded for 5 min at −50 mV, the potential was changed to +50 mV, Rs was verified, and a 5 min recording was then obtained at +50 mV, after which Rs was verified again. In some experiments, this procedure was repeated for further recording sessions at either potential, and Rs was checked between each session. Recordings were not analyzed if Rs increased more than twofold or reached 10 MΩ. Because the membrane capacitance was ~50 pF, this limited the recording bandwidth to 5 kHz, the filter cutoff frequency chosen during data acquisition.

Fast-flow recordings. Electrodes of 10–15 MΩ resistance were used to obtain a whole-cell configuration near the middle of deep muscle fibers; outside-out membrane patches were then isolated by slowly pulling the pipette off the cell. Fast-flow applications were performed as described previously (Legendre, 1998). The outside-out patch was positioned obliquely approximately 100 μm away from the stream of a twin-barreled application pipette, close to the interface formed between the solutions. One barrel contained control solution consisting of (in mM): NaCl 145, KCl 1.5, $CaCl_2$ 0.6, $MgCl_2$ 10, glucose 10, and HEPES 10, adjusted to pH 7.2, 330 mOsm. The other barrel contained ACh (0.1, 1, or 10 mM) dissolved in control solution. The solution exchange was performed by rapidly moving the solution interface across the tip of the patch pipette, using a piezo-electric translator (model P245.30, Physic Instruments). Current was recorded with an Axopatch-1D amplifier (Axon Instruments), filtered at 10 kHz (−3 dB), and stored using a digital tape recorder. Data were acquired with pClamp 6.0 software (Axon Instruments) by digitizing at 50 kHz and were analyzed off-line with Axograph 3.5 software (Axon Instruments). In control experiments, the rising phase of the pipette junctional current had a time to peak (20–80%) of 0.08 msec. However, the real exchange time results partially from an unstirred layer around the patch. The theoretical limit to the full exchange time was therefore estimated (Legendre, 1998) by assuming a patch diameter of 0.4–0.5 μm and found to be closer to 0.11 msec. Because the activation kinetics of AChRs can be as fast as our application technique, we obtained an estimate of the maximum activation time by applying a saturating concentration of agonist (10 mM ACh). The activation phase of the current evoked by 10 mM ACh application (20–80% rise time, 0.04 ± 0.01 msec; mean ± SD; $n = 10$; patch potential V_h, +50 mV) was faster than the junctional current and is likely to reflect the real kinetic values. To the contrary, the time course of the current evoked by 1 mM ACh was close to the solution exchange time, which therefore appears to limit the onset of the response.

RESULTS

AChR properties

When 10 mM ACh was applied at a positive potential (+50 mV), a step-like outward (upward) current appeared during the period of application (Fig. 1*A*). In contrast, when the same patch was held at a negative potential (−50 mV), a clear plateau of inward (downward) current (reversing near 0 mV) was evident during ACh application (labeled "1"). Upon removal of ACh, a large transient rebound current appeared (labeled "2"). At a lower ACh concentration of 1 mM (Fig. 1*B*), a smaller current was evoked at −50 mV compared with at +50 mV during ACh

application, and a small rebound current appeared immediately after ACh removal and then decayed to baseline. When only 0.1 mM ACh was applied, similar current steps were observed at +50 and −50 mV (Fig. 1*C*), presumably attributable to a lack of block at this concentration. The extent of current block was estimated from the difference between the peak rebound current after removal of ACh and the early plateau current level during ACh application. The block (summarized in Fig. 1*D*) was negligible (<5%) at 0.1 mM and at all ACh concentrations tested at +50 mV (*black bars*) but was increasingly obvious at higher ACh concentrations when the patches were held at −50 mV (*stippled bars*). For responses evoked by the application of 10 mM ACh, the block reached 79 ± 10% (n = 10), which presumably is limited by equilibration between the open and blocked states of the AChR (see below).

Other features of the currents were examined by comparing the activation and deactivation time courses observed under different conditions. At 10 mM ACh, the 20–80% rise time at −50 mV (Fig. 1*E*, *stippled bars*) was 0.04 ± 0.01 msec (n = 10) for the plateau current (1) and 0.05 ± 0.03 msec (n = 10) for the rebound current (2). These values were not significantly different from that measured at +50 mV (*black bar*; 0.04 ± 0.01 msec; n = 10; paired t test; $p > 0.05$). The rise times of the responses evoked by 1 mM ACh application and for both components of the responses evoked by 10 mM ACh were limited by the solution exchange time and recording bandwidth (see Materials and Methods). Application of 0.1 mM ACh (for 1 msec) evoked responses with a longer 20–80% rise time at both potentials (Fig. 1*E*), consistent with the slower activation of AChRs expected at this lower agonist concentration. The rise time was 0.17 ± 0.05 msec (n = 5) at V_h of −50 mV and 0.17 ± 0.07 msec (n = 5) at V_h of +50 mV. The deactivation time constant (τ_{off}) of responses evoked at this concentration had similar values at both negative (0.18 ± 0.03 msec; n = 5) and positive (0.17 ± 0.05 msec; n = 5) holding potentials (Fig. 1*F*), suggesting that, at this agonist concentration, zebrafish AChR closure after removal of ACh was voltage-independent. When V_h was +50 mV, τ_{off} of the responses evoked by the application of 10 mM ACh (0.20 ± 0.11 msec; n = 10) had similar values to those obtained when 0.1 mM ACh was applied. But at V_h of −50 mV, τ_{off} was significantly longer (0.30 ± 0.10 msec; n = 10) at the higher concentration (paired t test; $p < 0.05$) (Fig. 1*F*). This slower decay time of the rebound current obtained at negative potentials appears to be related to an additional delay in unbinding of ACh from open but blocked channels under these conditions (see below). A similar rebound of the ACh-evoked current during recovery from open channel block was also reported for AChRs from chromaffin cells (Maconochie and Knight, 1992a) and mouse muscle (Maconochie and Steinbach, 1998).

Open channel block

We examined the voltage dependence of the effect of 10 mM ACh in greater detail, as shown in Figure 2. ACh was applied for 1 msec at holding potentials ranging between +40 and −70 mV in this example. As the potential was held more negative, the early plateau current reached a limiting amplitude, whereas the rebound current became progressively larger (Fig. 2A). As shown in Figure 2*B*, the peak of the rebound current varied linearly over this potential range (*open circles*), whereas the steady current increased similarly at positive potentials but was reduced (rectified) at voltages of −20 mV or less (*filled circles*). The voltage dependence of the block was estimated as shown in Figure 2*C* in

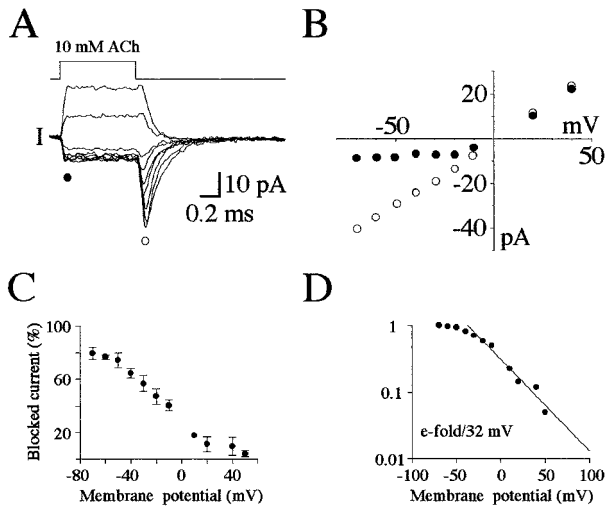

Figure 2. Voltage dependence of the effect of 10 mM ACh. *A*, Series of current responses evoked in the same patch upon exposure to 10 mM ACh at potentials of +40, +20, −10, −20, −30, −40, −50, −60, and −70 mV (from *top* to *bottom traces*; averages of 8 trials). The *filled circle* denotes the early plateau phase, and the *open circle* denotes the peak of the rebound phase. *B*, Plot of the current during the early plateau phase (*filled circles*) and peak of the rebound phase (*open circles*) at each potential examined for the traces shown in *A*. *C*, Summary of the difference between the peak rebound current and early plateau current (*Blocked current*), plotted as a percentage of the total current observed at each potential. SDs (n = 5) are indicated by the error bars. *D*, Same results as in *C* normalized for the maximal block (at −70 mV) on a logarithmic scale and plotted as a function of voltage. The *solid line* is the best linear fit of the foot of the curve and indicates an e-fold increase in block for a 32 mV hyperpolarization.

which the difference between the amplitudes of the peak of the rebound current and the early plateau current, normalized as a percentage of the peak current, is plotted at different holding potentials. The proportion of blocked current can be seen to increase as the voltage was decreased and reached a maximum of ~80% block at −70 mV. In Figure 2*D*, these results are plotted on semilogarithmic coordinates. The relationship between the extent of block (on a logarithmic scale) and the holding potential could be well fitted by a single exponential function (straight line) between −40 and +50 mV. Accordingly, the block increased with a limiting slope of e-fold/32 mV of hyperpolarization. A similar steady-state voltage dependence has been reported for block of BC3H1 clonal muscle cell AChRs by millimolar ACh (Liu and Dilger, 1991) and for local anesthetic block of AChRs in denervated frog muscle (Neher and Steinbach, 1978), and slightly lower voltage dependencies have been reported in other preparations (Ogden and Colquhoun, 1985; Sine et al., 1990). Therefore, ACh appears to bind to a site well within the membrane field in a variety of AChRs.

Because ACh is positively charged, it may enter and permeate the AChR as the pore discriminates only poorly between cations (Dwyer et al., 1980). At high (millimolar) concentrations of ACh, such as that reached in the synaptic cleft during neuromuscular transmission (Clements, 1996), a reversible block of the channels has been described previously (Sine and Steinbach, 1984; Ogden and Colquhoun, 1985; Sine et al., 1990; Liu and Dilger, 1991; Maconochie and Knight, 1992a; Maconochie and Steinbach, 1998). Similarly, open channel block has been observed in some AChRs by 5-hydroxytryptamine (Grassi et al., 1993), extracellular (Marty, 1980) and intracellular Mg^{2+} ions (Sands and Barish,

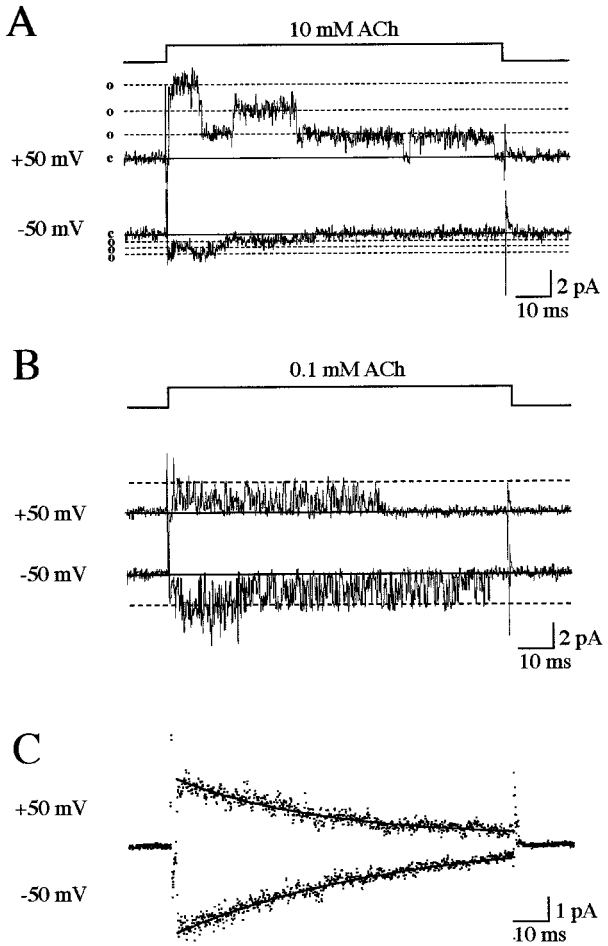

Figure 3. Open channel block by ACh. *A*, The *top line* indicates the 100 msec period of application of 10 mM ACh to a patch containing three AChRs. The *top trace* shows the current (filtered at 2 kHz) elicited during a single application at +50 mV. The baseline is indicated by *c* on the *left*; each of three consecutive open channel current levels are indicated by *o*. The *bottom trace* shows a response by the same patch during ACh application at −50 mV. Note the much smaller current amplitude. *B*, In contrast, the single channel current was insensitive to voltage when 0.1 mM ACh was applied to the same patch. *C*, Long pulses (100 msec) of 0.1 mM ACh also evoked a voltage-independent desensitization in this patch. In this example, 45 traces were averaged. At both voltages (+50 and −50 mV), the averaged trace decayed with a time course, which was well fitted by a single exponential curve with time constants (τ_d) of 43 msec at +50 mV and 64 msec at −50 mV.

1992; Ifune and Steinbach, 1991), and intracellular spermidine (Haghighi and Cooper, 1998). An open channel block of AChRs by ACh at negative voltages causes fast closures of the channel (Sine and Steinbach, 1984; Ogden and Colquhoun, 1985; Sine et al., 1990; Liu and Dilger, 1991; Maconochie and Knight, 1992a; Maconochie and Steinbach, 1998) with durations depending on the association and dissociation rates of the blocker within the pore. The presence of a rebound current for zebrafish AChRs, with an onset in the microsecond domain after agonist removal, predicts fast association and dissociation rates. If these kinetics exceed the bandwidth of the recordings, the block will be filtered and consequently reduce the single channel current, resulting in a flickering block as first described for open AChR block by local anesthetics (Neher and Steinbach, 1978). This was effectively the case as shown in Figure 3*A* for a patch with at least three channels. In this example, a 100 msec application of 10 mM ACh evoked single channel activity with an apparent approximate fourfold lower single channel current amplitude at negative potentials because of the flickering block. At a positive potential (*top trace*), we observed occasional long-lasting closures, which eventually terminated the current as a result of slow desensitization (see below). When ACh was applied to the same patch at a lower concentration of 0.1 mM (Fig. 3*B*), we observed better resolved current transitions because of slower, less filtered channel openings and closures at this lower concentration, and the amplitudes were similar at both potentials. These observations confirm that an open channel block occurred at high ACh concentrations and at negative potentials.

A 100 msec application of a low or high concentration of agonist also revealed a desensitization process characterized by a progressive decrease in single channel activity with time. Desensitization was nearly complete by 100 msec and is the reason a rebound current is not observed in Figure 3. The time course of desensitization is shown more clearly in Figure 3*C* for averaged currents evoked in the same patch with 0.1 mM ACh. The desensitization time constant (τ_d) appeared to be independent of the voltage and ACh concentration at the levels tested. The values of τ_d at 0.1 mM ACh were 53 ± 10 msec ($n = 7$) at +50 mV and 51 ± 5 msec ($n = 7$) at −50 mV; at 10 mM ACh, they were 43 ± 14 msec ($n = 7$) at +50 mV and 45 ± 15 msec ($n = 10$) at −50 mV. These values did not differ significantly (paired *t* test; $p > 0.05$). The desensitization process was therefore too slow to participate significantly in the phenomena occurring during brief (1 msec) applications, and paired-pulse experiments confirmed this point (data not shown).

Kinetic model of the AChR and mEPC time course

A simple kinetic model of the AChR with a blocked "open" channel state can well describe our main results of concentration-dependent (Fig. 4*A*) and voltage-dependent (Fig. 4*B*) block by ACh. This model was originally proposed for chromaffin AChRs (Maconochie and Knight, 1992b). The rate constants were chosen based on our experimental data and on detailed kinetic studies of AChRs performed in other preparations. We assumed two equivalent closed states that each bind ACh and rapidly interconvert, as described for muscle AChRs in other species (Colquhoun and Sakmann, 1985; Auerbach and Lingle, 1987; Colquhoun and Ogden, 1988; Sine et al., 1990; Liu and Dilger, 1991), leading to opening of the doubly occupied receptor and subsequent concentration- and voltage-dependent block by ACh.

Explicitly, the mechanism of block of zebrafish AChRs can be well described by the following linear kinetic model in which *A* denotes a molecule of ACh:

Forward: $2k_{on}$ k_{on} β b

$$3A + C \leftrightarrow 2A + AC \leftrightarrow A + A_2C \leftrightarrow A + A_2O \leftrightarrow A_3B$$

Backward: k_{off} $2k_{off}$ α r

For simplicity, we assumed two identical, interconnected binding states (C and AC) with an optimum forward rate constant (k_{on}) of 1.6×10^8 M^{-1} sec^{-1} and an optimum dissociation rate constant (k_{off}) of 9×10^3 sec^{-1}. This is close to that previously proposed for muscle AChRs (Colquhoun and Sakmann, 1985; Auerbach and Lingle, 1987; Colquhoun and Ogden, 1988; Sine et al., 1990; Liu and Dilger, 1991). The value of k_{off} was adjusted depending on k_{on} to limit reopening of the channel as suggested by the fast deactivation phase of the outside-out currents we observed (Fig.

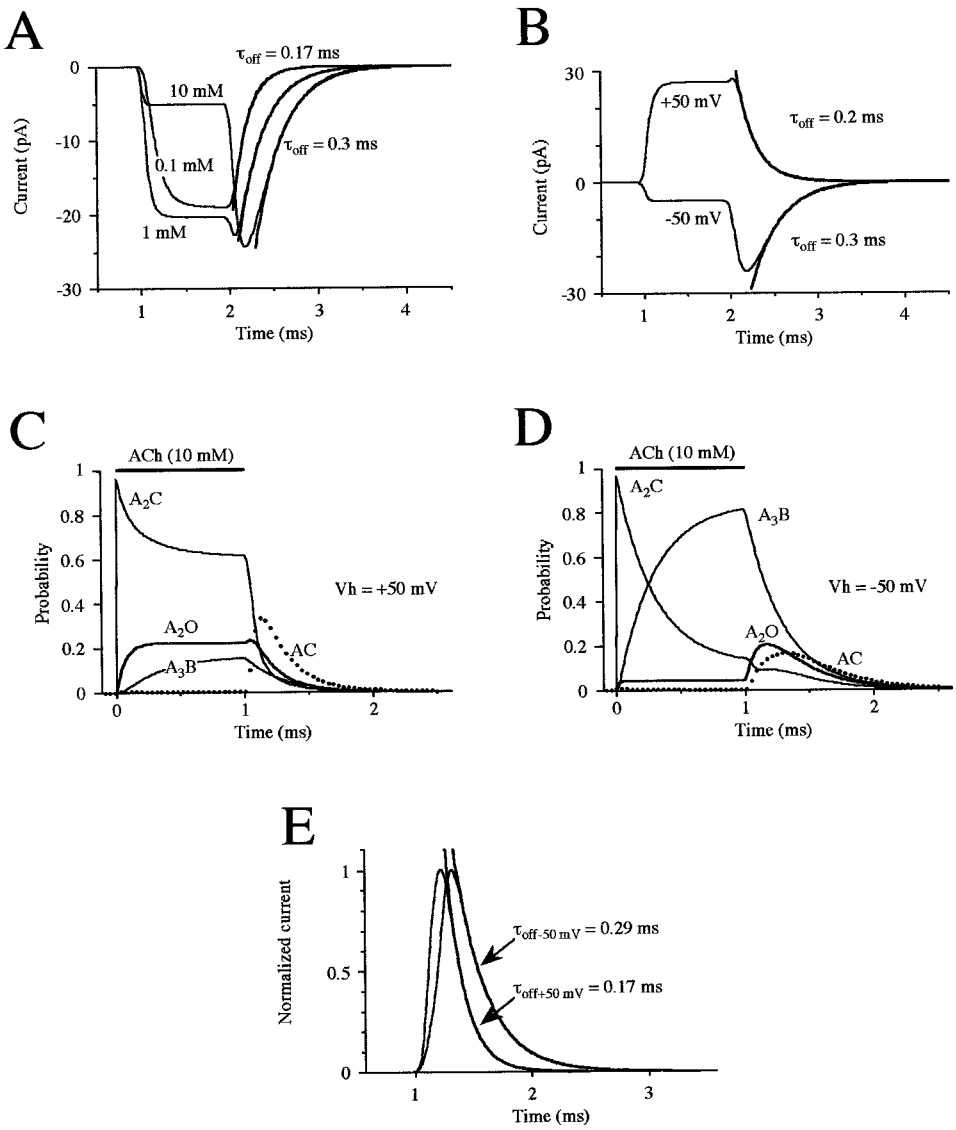

Figure 4. Model of AChRs and predicted properties of mEPCs during open channel block. *A*, Model predictions of the effects of a 1 msec application of 0.1, 1, and 10 mM ACh (as indicated). The *solid curves* are exponential fits of the current decay after application of 0.1 and 10 mM with the indicated time constants. *B*, Model prediction of the voltage dependency of open channel block evoked by ACh (10 mM applied for 1 msec) at +50 and −50 mV. The *solid curves* are exponential fits of the current decay at either potential with the indicated time constants. Model prediction of the evolution of the kinetic states during a 1 msec application of 10 mM ACh at +50 (*C*) and −50 (*D*) mV. Each *trace* represents a different state: monoliganded (*AC*) and diliganded closed states (A_2C), the open channel (A_2O), and the blocked channel (A_3B). *E*, Prediction of the time course of the mEPC at −50 and +50 mV elicited by a 0.125 msec duration pulse of 10 mM ACh. The mEPCs are scaled to a similar peak. The *solid curves* are exponential fits of the mEPC decay at either potential with the indicated time constants. The rise times were 0.08 msec at +50 mV and 0.12 msec at −50 mV.

1*F*), but the exact values chosen were not as critical as the values of the other rate constants in the model. The doubly bound closed state (A_2C) led to an open state (A_2O) with an open rate constant (β) of 3.5×10^3 sec^{-1}, similar to that proposed for the AChR of the frog (Colquhoun and Sakmann, 1985). The estimated closing rate constant (α) needed to be faster (9.5×10^3 sec^{-1}) to obtain a fast rise time and decay time constant. A fast rate for α has also been observed in high-resolution stationary kinetic analyses of AChRs at high (>0.1 mM) ACh concentrations (Sine et al., 1990). As for other muscle AChRs (Sine and Steinbach, 1984; Ogden and Colquhoun, 1985; Sine et al., 1990; Liu and Dilger, 1991; Maconochie and Knight, 1992a; Maconochie and Steinbach, 1998), we propose that the open state was blocked (A_3B) by ACh with an essentially diffusion-limited rate constant (b) estimated as 7×10^6 M^{-1} sec^{-1}. To predict the voltage dependence of the mechanism of block, b was set using the relationship $b \times \exp -[(V_h + 50\ mV)/30\ mV]$ so that the block decreased e-fold/30 mV depolarization, which gave a somewhat better fit than the value of e-fold/32 mV observed experimentally (Fig. 2*D*). The recovery rate constant (r) was estimated as 3.5×10^3 sec^{-1} at −50 mV, which is an order of magnitude slower than the recovery rate estimated for other AChRs. This indicates a more stable blocked state that results in a prolonged recovery (rebound) phase.

It was critical that the value of r should be close to that of β to yield a flat plateau phase during the block, followed by a more slowly decaying and voltage-dependent current during the recovery phase. However, the rise time calculated for application of 10 mM ACh was approximately twice that observed with outside-out patches (Fig. 1*E*,*F*). Increasing the values of β and r yielded more appropriate rise times, but the decay rate became voltage- and concentration-independent. In the absence of more direct information on activation kinetics in the microsecond domain, we compromised the model by allowing for slightly slower rise times while retaining the essential biophysical and physiological features (see below) of the block. These features include a slowing of the deactivation phase at higher ACh concentrations (Fig. 4*A*) and at hyperpolarized compared with depolarized potentials (Fig. 4*B*), which resemble the rebound current observed experimentally (Figs. 1*A*,*F*, 2*A*). Desensitization was not taken into account because it was too slow (Fig. 3*C*) to shape the time course of the current evoked by a short pulse of ACh. We rejected other models, such as multiple blocking sites (Maconochie and Stein-

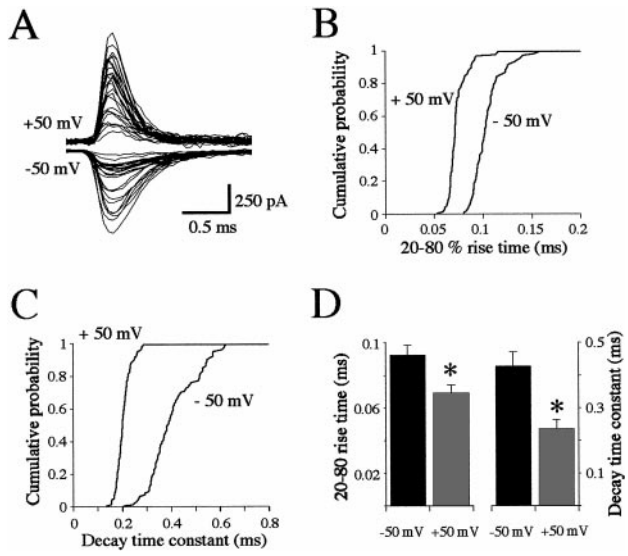

Figure 5. Properties of mEPCs recorded *in vivo*. *A*, Overlap of 25 mEPCs recorded from the same muscle fiber at +50 (*top traces*) and −50 (*bottom traces*) mV. Cumulative histograms of the 20–80% rise times (*B*) and monoexponential decay time constants (*C*) for all events recorded at +50 ($n = 99$) and −50 ($n = 85$) mV. *D*, Summary histogram of the values obtained in all ($n = 15$) recordings. The mean ± SD for the rise times (*left*) and decay time constants (*right*) at −50 (*black bars*) and +50 (*gray bars*) mV. The *asterisks* indicate significance at $p < 0.01$.

bach, 1998), interconversion between blocked and closed states, or a second open state reached from the monoliganded state, because these failed to account for the slowing of the decay time constant.

The role of open channel block in the single channel current behavior is indicated more clearly in Figure 4, *C* and *D*. Here, we have plotted the evolution predicted for different states of the channel during a 1 msec application of 10 mM ACh with minimal block at +50 mV (Fig. 4*C*) and with a strong block at −50 mV (Fig. 4*D*). During ACh application at +50 mV (Fig. 4*C*), the monoliganded state (*AC*) is almost entirely dissipated as the diliganded state (A_2C) is rapidly reached at the onset of the application, resulting in ~25% of channels opening (A_2O) after a similar, rapid time course. In addition, a somewhat smaller fraction (~15%) of the channels become blocked (A_3B) after a slower time course. Removal of the ACh results in dissipation of the diliganded closed and open states and a delayed, transient appearance of the monoliganded closed. Reversal of the block contributes only a small peak (<5%) of open channels at the onset, as observed experimentally (Fig. 1*A*,*D*), and the blocked channels recover at a similar rate as the closing of the open channels (Fig. 1*F*).

During application of ACh at −50 mV resulting in strong open channel block (Fig. 4*D*), the monoliganded closed state is again essentially entirely dissipated as the diliganded closed state is rapidly reached at the onset of the application. However, the diliganded closed state declines to a much greater extent and results in a smaller fraction (<5%) of openings because of a large accumulation of blocked channels. Removal of the ACh results in immediate reversal of channel block and a delayed opening of the channels, which consequently close at a slower rate than observed in the absence of block. Closing of the channels sustains the (initially more rapid) decline of the diliganded closed state and results in the further delayed and transient appearance of the monoliganded closed state. It can be seen that at this potential that the openings are generated mostly from blocked channels.

Properties of mEPCs

Based on this model, we predicted the time course of mEPCs expected at +50 and −50 mV (Fig. 4*E*) i.e., with weak and strong open channel block. We assumed for simplicity that ACh is released instantaneously into the synaptic cleft as a brief, square pulse (duration of 0.125 msec) at a concentration of 10 mM. This resulted in mEPCs with rise times comparable with those observed experimentally (data for unfiltered events taken from Nguyen et al., 1999, and see below). The mEPCs predicted at V_h of −50 mV were somewhat lower in amplitude (by ~25%) than those predicted at +50 mV (see Fig. 6*C*; scaled to the same amplitude in Fig. 4*E*), and both their rise time and decay time courses were slower. These differences in the mEPCs predicted at the two potentials result from the reduction in channel current amplitude and slowing of the rebound current described above for the single channel recordings.

We then examined the properties of mEPCs recorded *in vivo* at these two potentials to see whether similar differences occur. In the presence of TTX and a low Ca–high Mg solution, quantal mEPCs at either potential fluctuated highly in amplitude, as we reported previously in recordings at physiological potentials (Nguyen et al., 1999). We suggested that the lack of a simple, gaussian distribution of mEPC amplitudes was caused by the polyinnervation of zebrafish muscle cells by both primary and secondary motoneurons (Myers, 1985; Westerfield et al., 1986). Because our model predicted a limited reduction in amplitude at −50 mV compared with +50 mV, we were unable to detect this effect given the larger experimental variability. Individual events at a given potential had a relatively homogenous time course (Fig. 5*A*). Cumulative histograms of individual mEPC rise times (Fig. 5*B*) and decay time constants (Fig. 5*C*) from a representative experiment clearly show that both values were larger at the hyperpolarized, blocking potential. These observations were significant for all ($n = 15$) experiments (Fig. 5*D*) and suggest that a strong open channel block occurs during ACh release under physiological conditions and that its reversal contributes most of the mEPC.

To examine the physiological implications of the block in greater detail, we predicted the effects of gradually varying several parameters of the kinetic model on the properties of the mEPCs calculated at +50 and −50 mV. Increasing the duration (from 0.05 to 0.50 msec) of the ACh pulse eliciting the mEPC resulted in a small but progressive increase in the decay time constant (Fig. 6*A*), but this remained slower at −50 mV compared with +50 mV. At an ACh concentration of 0.1 mM, the mEPC decay time constant was similar at the two potentials but became slower at −50 mV as the concentration increased (Fig. 6*B*); above 2 mM, the relative difference in the time constants became more constant, reaching a twofold difference at 10 mM. This difference is comparable with that observed *in vivo* (Fig. 5*D*), indicating that millimolar concentrations of ACh are present in the cleft during the mEPC, as observed at other NMJs and for other transmitters (Clements, 1996). At submillimolar concentrations of ACh the peak amplitude of the mEPC rose rapidly at both potentials, but at millimolar concentrations it became consistently smaller at −50 mV because of the block (Fig. 6*C*). At millimolar ACh concentrations, the reduction of the mEPC amplitude at −50 mV thus seemed to be offset by the prolongation of the decay time constant described above. To further examine

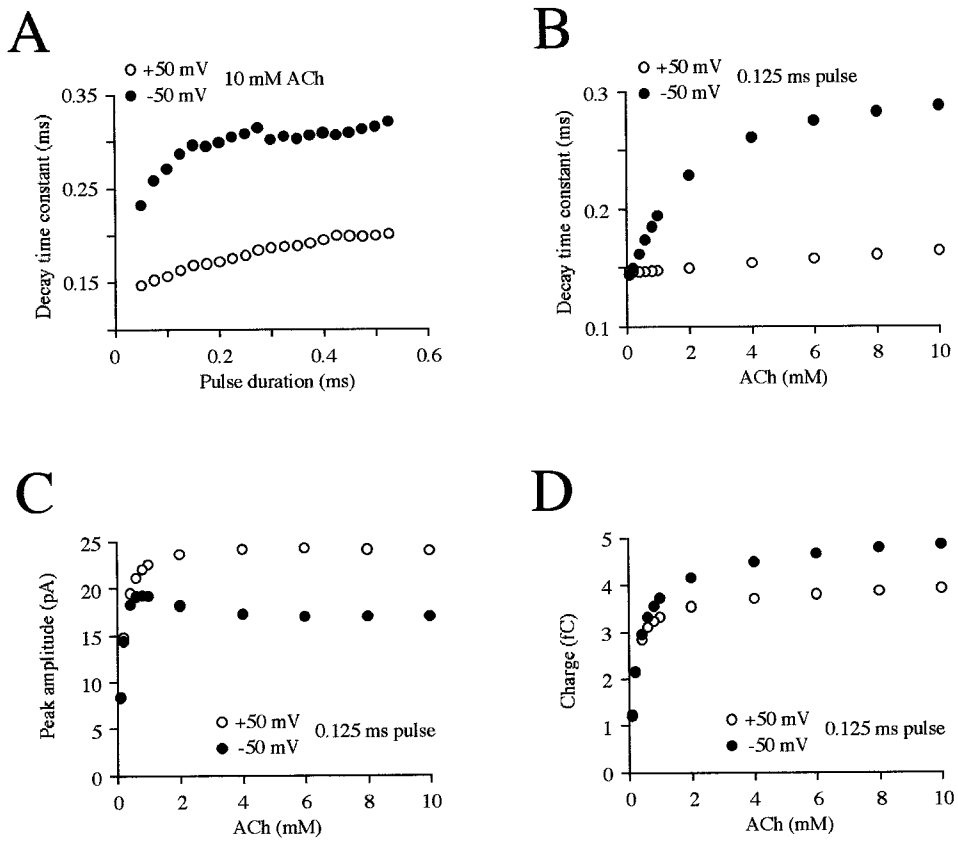

Figure 6. Effects of model parameters on predicted properties of the mEPC. *A*, Decay time constants are plotted as a function of the duration of a square pulse of 10 mM ACh. The values for the durations are incremented by 0.025 msec from 0.050 to 0.525 msec at −50 (*filled symbols*) and +50 (*open symbols*) mV. Effects of the ACh concentration on decay time constants (*B*), peak amplitudes (*C*), and charge (*D*) during a 0.125 msec pulse. The concentrations are 0.1, 0.2, 0.4, 0.6, 0.8, 1, 2, 4, 6, 8, and 10 mM.

this balance of mEPC properties, we estimated the charge contributed by the mEPC at each potential as the product of the amplitude and time constant predicted at each ACh concentration as shown in Figure 6, *B* and *C*, respectively. It can be seen in Figure 6*D* that the estimated charge rose rapidly with the ACh concentration at both potentials but was consistently greater at millimolar concentrations at −50 mV. This indicates that, despite the reduction in current amplitude because of the block, the delayed reversal of the block results in a prolonged current that allows more charge to enter the muscle cell at physiological potentials.

DISCUSSION

AChR properties

We observed a voltage-dependent block of AChRs during application of millimolar concentrations of ACh, followed by a rapid, rebound current upon removal of ACh. Open channel block of muscle AChRs by ACh has been observed in a variety of preparations in which the block was supposed to reduce the synaptic current as estimated from the results obtained during stationary kinetic measurements (Ogden and Colquhoun, 1985). In our nonstationary analysis, we observed a rebound current after removal of ACh, suggesting that, although a block occurs initially, a current can nevertheless be generated during recovery from the block. In fact, the same maximal conductance was observed at positive potentials in which a sustained current (with minimal block) was generated during brief application and at negative potentials at the peak of the rebound (linear *I–V* relationship of Fig. 2*B*, *open circles*). This demonstrates that all of the activated channels can eventually generate a maximal current, even if they are initially blocked. Although the block does not modify the effectiveness of the channels, its reversal determines the time course of the response to ACh.

A rebound current was observed during nonstationary analysis of chromaffin cell AChRs (Maconochie and Knight, 1992a) in which the physiological significance remains unclear and for cloned mouse muscle AChRs (Maconochie and Steinbach, 1998). For zebrafish AChRs, we estimated similar association, dissociation, opening, and block onset rate constants as for most other muscle AChRs (Sine and Steinbach, 1984; Ogden and Colquhoun, 1985; Colquhoun and Sakmann, 1985; Auerbach and Lingle, 1987; Colquhoun and Ogden, 1988; Sine et al., 1990; Liu and Dilger, 1991). Our value for the closing rate ($\alpha = 9500\ \text{sec}^{-1}$) is among the highest reported, e.g., as for torpedo AChRs (8000 sec^{-1}) (Sine et al., 1990). However, the unblocking rate (r) was estimated to be an order of magnitude slower than for other AChRs, accounting for the prolonged effect observed with the otherwise fast AChR kinetics described here.

End plate currents

We were able to simulate (data not shown) a synaptic-like rebound current using the rate constants for previously published studies of muscle AChR (Sine and Steinbach, 1984; Ogden and Colquhoun, 1985; Liu and Dilger, 1991; Maconochie and Knight, 1992a; Maconochie and Steinbach, 1998), including the *Torpedo* electroplax (Sine et al., 1990). This suggests that recovery from open channel block is a ubiquitous component of synaptic transmission at the NMJ that plays a more important role at synapses in which the unblocking rate is closer to the channel activation rate. The slow unblocking rate estimated for the zebrafish AChR together with the lack of channel reopenings result in the reversal of block being the major determinant of the decay time course of

the mEPC. At other NMJs with faster unblocking rates and longer mean open times, consisting of bursts with multiple reopenings, the block may slow the first opening in a burst (when the blocking ACh molecule rapidly dissociates) but not later openings. Under these conditions, the block would have a minimal effect on the mean channel open time and consequently the mEPC duration. An additional factor in determining the end plate current time course is ACh diffusion (Bartol et al., 1991), particularly when multiple quanta are secreted during evoked release at NMJs with extended postsynaptic receptor matrices.

We conclude that, at larval zebrafish end plates, ACh is rapidly released at millimolar concentrations and blocks the AChRs as soon as they open. It is important to stress that the AChRs are rapidly blocked by millimolar concentrations of ACh because this prevents the membrane from depolarizing during vesicle release under physiological conditions, which otherwise would reduce the effect of the block. Once ACh is removed from the cleft, bound ACh slowly leaves the pore of the blocked channels, and a transient, synaptic current is generated by reversal of open channel block. Millimolar concentrations of transmitter have been estimated at a number of synapses, including NMJs and central synapses (Clements, 1996). A variety of kinetic mechanisms are thought to define the decay time course of synaptic events, ranging from fast to slow desensitization and simple closure of the channels after clearance of transmitter (Jones and Westbrook, 1996). The reversal of open channel block that we observed is a novel mechanism of synaptic transmission. The delayed appearance of the ACh-evoked current (because of recovery from block) is reminiscent of the presynaptic calcium tail current (because of calcium channel closure) that is delayed until the repolarization phase of the action potential (Llinas et al., 1982). It is thus paradoxical that, at the zebrafish NMJ, much of the action appears to take place after rather than during the stimuli.

Physiological significance of open channel block

According to our model simulations, the duration of the synaptic current is not particularly sensitive to variations in the duration of ACh exposure (e.g., 0.05–0.50 msec) whether or not a block occurs (Fig. 6*A*). In contrast, the duration of the rebound current is far more sensitive to variations in the peak concentration of ACh. At lower ACh concentrations the time course of the synaptic current is limited mainly by the rate of activation and deactivation of the AChRs, whereas at higher concentrations the rebound current is determinant. At the zebrafish NMJ, the time course of the postsynaptic response should therefore be potentiated when higher concentrations of ACh are released into the synaptic cleft. This potentiation could be significant during development because of variations in the extent of synaptic maturation and at mature synapses after multivesicular release evoked by a presynaptic action potential. Reversal of open channel block could thus serve as a simple and reliable biophysical mechanism to prolong the time course of synaptic transmission and thus enhance the postsynaptic action of ACh. We speculate that this may also be the case at the *Torpedo* electroplax and at other NMJs and may be especially important at those in which the rate of decay of mEPCs is related to the rate of muscle contractions (Dionne and Parsons, 1978, 1981; Miledi and Uchitel, 1981).

Although the block slows the time course of the mEPC, the amplitude is also predicted to be reduced. However, our estimates of the synaptic charge suggest that the former outweighs the latter. The efficacy of the NMJ is usually thought to be a direct consequence of the depolarization produced at the single, discrete end plate. However, zebrafish muscle cells are polyinnervated, with tiny synapses contributed by each motoneuron (Liu and Westerfield, 1992) and thus more closely resembling immature NMJs in other species. Because the small synapses are spread over the surface of each muscle fiber, we suggest that the greater charge generated by reversal of open channel block allows for a better distribution of the depolarization along the equivalent cable of the muscle cell. This mechanism would be thus be more akin to synaptic activation of neurons in which distant synapses are thought to be integrated by dendritic cable properties (Rall, 1969).

REFERENCES

Auerbach A, Lingle CJ (1987) Activation of the primary kinetic modes of large- and small-conductance cholinergic ion channels in *Xenopus* myocytes. J Physiol (Lond) 393:437–466.

Bartol TM, Land BR, Salpeter EE, Salpeter MM (1991) Monte Carlo simulation of miniature endplate current generation in the vertebrate neuromuscular junction. Biophys J 59:1290–1307.

Clements JD (1996) Transmitter timecourse in the synaptic cleft: its role in central synaptic function. Trends Neurosci 19:163–167.

Colquhoun D, Ogden DC (1988) Activation of ion channels in the frog end-plate by high concentrations of acetylcholine. J Physiol (Lond) 395:131–159.

Colquhoun D, Sakmann B (1985) Fast events in single-channel currents activated by acetylcholine and its analogues at the frog muscle endplate. J Physiol (Lond) 369:501–557.

Dionne VE, Parsons RL (1978) Synaptic channel gating differences at snake twitch and slow neuromuscular junctions. Nature 274:902–904.

Dionne VE, Parsons RL (1981) Characteristics of the acetylcholine-operated channel at twitch and slow fibre neuromuscular junctions of the garter snake. J Physiol (Lond) 310:145–158.

Dwyer TM, Adams DJ, Hille B (1980) The permeability of the endplate channel to organic cations in frog muscle. J Gen Physiol 75:469–492.

Eaton RC, Farley RD, Kimmel CB, Schabtach E (1977) Functional development in the Mauthner cell system of embryos and larvae of the zebra fish. J Neurobiol 8:151–172.

Fatt P, Katz B (1952) Spontaneous subthreshold activity at motor nerve endings. J Physiol (Lond) 117:109–128.

Grassi F, Polenzani L, Mileo AM, Caratsch CG, Eusebi F, Miledi R (1993) Blockage of nicotinic acetylcholine receptors by 5-hydroxytryptamine. J Neurosci Res 43:562–570.

Haghighi AP, Cooper E (1998) Neuronal nicotinic acetylcholine receptors are blocked by intracellular spermine in a voltage-dependent manner. J Neurosci 18:4050–4062.

Hamill OP, Marty A, Neher E, Sakmann B, Sigworth FJ (1981) Improved patch-clamp techniques for high-resolution current recording from cells and cell-free membrane patches. Pflügers Arch 391:85–100.

Ifune CK, Steinbach JH (1991) Voltage-dependent block by magnesium of neuronal nicotinic acetylcholine receptor channels in rat phaeochromocytoma cells. J Physiol (Lond) 443:683–701.

Jones MV, Westbrook GL (1996) The impact of receptor desensitization on fast synaptic transmission. Trends Neurosci 19:96–101.

Legendre P (1998) A reluctant gating mode of glycine receptor channels determines the time course of inhibitory miniature synaptic events in zebrafish hindbrain neurons. J Neurosci 18:2856–2870.

Legendre P, Korn H (1994) Glycinergic inhibitory synaptic currents and related receptor-channel in the zebrafish brain. Eur J Neurosci 6:1544–1557.

Liu DWC, Westerfield M (1988) Function of identified motoneurons and co-ordination of primary and secondary motor systems during zebrafish swimming. J Physiol (Lond) 403:73–89.

Liu DWC, Westerfield M (1992) Clustering of acetylcholine receptors requires motoneurons in live embryos, but not in cell culture. J Neurosci 12:1859–1866.

Liu Y, Dilger JP (1991) Opening rate of acetylcholine receptor channels Biophys J 60:424–432.

Llinas R, Sugimori M, Simon SM (1982) Transmission by presynaptic spike-like depolarization in the squid giant synapse. Proc Natl Acad Sci USA 79:2415–2419.

Maconochie DJ, Knight DE (1992a) A study of the bovine adrenal chromaffin nicotinic receptor using patch clamp and concentration-jump techniques. J Physiol (Lond) 454:129–153.

Maconochie DJ, Knight DE (1992b) Markov modelling of ensemble current relaxations: bovine adrenal nicotinic receptor currents analysed. J Physiol (Lond) 454:155–182.

Maconochie DJ, Steinbach JH (1998) The channel opening rate of adult- and fetal-type mouse muscle nicotinic receptors activated by acetylcholine. J Physiol (Lond) 506:53–72.

Marty A (1980) Action of calcium ions on acetylcholine-sensitive channels in *Aplysia* neurones. J Physiol (Paris) 76:523–527.

Miledi R, Uchitel OD (1981) Properties of postsynaptic channels induced by acetylcholine in different frog muscle fibres. Nature 291:162–165.

Myers PZ (1985) Spinal motoneurons of the larval zebrafish. J Comp Neurol 236:555–561.

Neher E, Steinbach JH (1978) Local anaesthetics transiently block currents through single acetylcholine-receptor channels. J Physiol (Lond) 277:153–176.

Nguyen PV, Aniksztejn L, Catarsi S, Drapeau P (1999) Neuromuscular transmission during early development of the zebrafish. J Neurophysiol 81:2852–2861.

Ogden DC, Colquhoun D (1985) Ion channel block by acetylcholine, carbachol and subderyldicholine at the frog neuromuscular junction. Proc R Soc Lond B Biol Sci 225:329–355.

Rall W (1969) Time constants and electronic lengths of membrane cylinders and neurons. Biophys J 9:1483–1508.

Saint-Amant L, Drapeau P (1998) Time course of the development of motor behaviors in the zebrafish embryo. J Neurobiol 37:622–632.

Sands SB, Barish ME (1992) Neuronal nicotinic acetylcholine receptor currents in phaeochromocytoma (PC12) cells: dual mechanisms of rectification. J Physiol (Lond) 447:467–487.

Sine SM, Steinbach JH (1984) Agonists block currents through acetylcholine receptor channels. Biophys J 46:277–284.

Sine SM, Claudio T, Sigworth FJ (1990) Activation of *torpedo* acetylcholine receptors expressed in mouse fibroblasts. J Gen Physiol 96:395–437.

Westerfield M, McMurray JV, Eisen JS (1986) Identified motoneurons and their innervation of axial muscles in the zebrafish. J Neurosci 6:2267–2277.